Research Article

Octavian-Gabriel Simionescu*, Cristina Pachiu, Octavian Ionescu, Niculae Dumbrăvescu, Octavian Buiu, Radu Cristian Popa, Andrei Avram, and Gheorghe Dinescu

Nanocrystalline graphite thin layers for low-strain, high-sensitivity piezoresistive sensing

https://doi.org/10.1515/rams-2020-0031
Received Jan 29, 2020; accepted May 22, 2020

Abstract: Bulk nanocrystalline graphite has been investigated as a possible candidate for piezoresistive sensors. The thin films were grown using capacitively coupled plasma enhanced chemical vapor deposition and a technological workflow for the transfer of the active material onto flexible substrates was established in order to use the material as a piezoresitive element. Preliminary electrical measurements under mechanical strain were performed in order to test the piezoresistive response of the material and promising GF values of 50 – 250 at 1% strain were obtained.

Keywords: flexible sensors, film transfer, gauge factor

1 Introduction

Piezoresistive sensing relies on measuring the relative variation of an electrical resistance $\left(\frac{\Delta R}{R}\right)$ with respect to the applied mechanical strain $\left(\varepsilon = \frac{\Delta l}{l}\right)$. The proportionality factor between these relative quantities represents the sensor sensitivity, termed as gauge factor (GF). Piezoresistive sensors are actively studied for a multitude integrated low-strain or high-strain sensing applications, such as: structural health monitoring for various industries [1–3]; pressure, inertial or cantilever MEMS [4]; as wearable electronics for personalized health management by heartbeat, arterial pressure or respiratory rate monitoring [3, 5–8]; touch/tactile sensors, motion detection and gesture registration for man-machine interactions [3, 5–7, 9–11]. The common commercially available piezoresistive sensors are known as foil strain gauges and consist of a patterned metallic film or a semiconductor bar exhibiting GFs around 2, or 100, respectively. Alternative materials and architectures are currently studied to improve sensitivity and stability. Based on good and stable conductivity and favorable chemistry and structure, graphene and other carbon-based composites and structures represent one of the most pursued paths.

Graphene and graphene derived materials show great promise for strain sensing, usually based on a combination between intrinsic, and inter-particle resistance variation. Recent studies report GF values of: ~6.1 for low-strain sensing, using chemical vapor deposition (CVD) graphene transferred from a metal catalyst to polydimethylsiloxane (PDMS) [12]; ~2 for strains up to 30% using buckled nanographene on PDMS [13]; ~11.4 for a graphene/epoxy composite [14]; ~1.9 for suspended graphene up to 3% strain [15]; from ~1143.5 to ~20.9 for 1 to 7 bilayers (BL) of graphene nanoplatelets (GNP), respectively, assembled layer by layer on a PDMS substrate at a strain of 5%, and ~301.61-29631 for a grid patterned 3 BLs of GNP at 10%-25% strains [6]; ~457 for laser induced graphene (LIG) encapsulated in a flexible polymer at strains up to 35% [7]; ~112 through direct laser writing (DLW) of porous graphitic structures on polyimide films [3]; ~125 for inkjet printed graphene [16]; of ~20 for strains to 1% and of ~40 for strains higher than 1.5% in the case of LIG on Kapton films [8]; and of ~2900 in the case of an individual single walled carbon nanotube (SWCNT) [17]. Although graphene and SWCNTs present extraordinary electrical conductivity, chemical stability and mechanical durability, they fall behind in regard to large-scale production and integration.

In this context, large area directly grown and conventionally processable thin layers of nanocrystalline

***Corresponding Author: Octavian-Gabriel Simionescu:** National Institute for Research and Development in Microtechnologies - IMT Bucharest, 126A Erou Iancu Nicolae Street, Voluntari city, Ilfov county, 077190, Romania; Faculty of Physics, University of Bucharest, 405 Atomistilor Street, Magurele city, Ilfov county, 077125, Romania; Email: octavian.simionescu@imt.ro
Cristina Pachiu, Octavian Ionescu, Niculae Dumbrăvescu, Octavian Buiu, Radu Cristian Popa, Andrei Avram: National Institute for Research and Development in Microtechnologies - IMT Bucharest, 126A Erou Iancu Nicolae Street, Voluntari city, Ilfov county, 077190, Romania
Gheorghe Dinescu: National Institute for Laser, Plasma and Radiation Physics, 409 Atomistilor Street, Magurele city, Ilfov county, 077125, Romania; Faculty of Physics, University of Bucharest, 405 Atomistilor Street, Magurele city, Ilfov county, 077125, Romania

graphite/graphene (NCG) may represent a sustainable alternative for low-strain, high-sensitivity applications (such as micro-fissure and structural vibration detection for railways, bridges, buildings, industrial machineries and in the automotive or aerospace industry) and recent studies have shown it can reach GF values of ~300 [18] and ~600 for strains up to 1% [10], values that surpass even those reported to date for strain sensing based on laser induced, or direct laser written graphite/graphene layers.

Plasma enhanced chemical vapor deposition (PECVD) is one of the most used techniques for the synthesis of NCG films. This method offers a great degree of control and fine tuning by providing a large number of process parameters to be adjusted [19–22]. Although the intimate morphology of the PECVD-synthesized material is yet to be established, various characterizations show that nanocrystalline graphite consists of nanodomains of sp^2 hybridized carbon atoms delimited by lattice mismatches, amorphous carbon or other defects. NCG can be seen as a broader class, as it can be further categorized in subclasses based on morphology and structure. A proposed nomenclature for the diversified carbonic structures can be consulted in [23]. While respecting the aforementioned nomenclature as much as possible and considering its various characterizations [24–26], we define the material used in this work as bulk-NCG: a thick and hard carbonic film consisting of 3D randomly orientated, graphite nanocrystals with a dominant turbostratic packing [27]

Thin films belonging to the broad class of NCG [27] have shown promise in applications such as: field emission [28], electrochemical sensing [25, 29, 30], photodetection [31, 32], nanoelectromechanical (NEM) switching [19], fabrication of microelectromechanical (MEM) resonators [20], protective coating [33] or gas separation [34]. The inhomogeneous conductive pathways formed by the sp^2 domains provide the material with a special functionality and a high conductivity response to small strains [10, 18, 35]. Zhao et al. [18] believe that the piezoresistive effect in NCG-type materials has a tunneling conduction support, similar to the mechanism characteristic to conductive polymer composites, where the play between the onset of electrical and geometrical connectivities of the filler particles is modulated by the quantum conduction through the thin acute gap formed in-between. The same group further modified their growth process - based on remote plasma-enhanced chemical vapor deposition (RPECVD) - to attain measurable conductivities even for thinner (more strain sensitive) NCG films [10]. They obtained significant sensitivity enhancement by increasing the substrate temperature (from 525°C to 600°C) during the plasma process and, in accordance with the assumed tunneling based sensing mechanism, concluded that the key to that enhancement was the higher nucleation density, lower grain size and larger initial tunneling distance that resulted thereby. It is indeed known the beneficial effect of a higher substrate temperature on the film nucleation density [19, 27, 36].

For the present stage of our strain sensor development we employed these findings, choosing to concentrate on both developing a consistent transfer process, and using a low resistance sensing film. Accordingly, we have per-

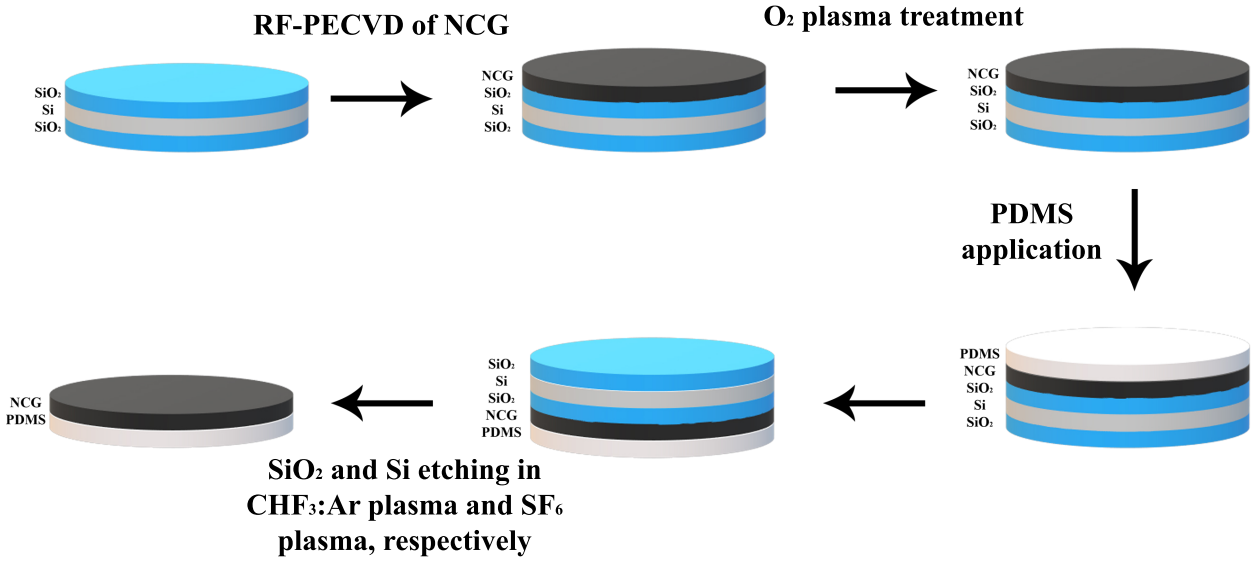

Figure 1: Schematic representation of the technological workflow

Table 1: NCG growth parameters

Step	Time t (min)	Heating speed (°/min)	Temperature T (°)	Pressure p (Pa)	RF power P_{RF} (W)	Gas flow (sccm) Ar	H_2	CH_4
Heat-up	-	15	200 ↗ 890	40	-	1500	200	-
Cleaning	0.5	-	890	200	-	1500	200	-
Growth	120	-	890	200	100	-	75	60
Post plasma processing	0.5	-	890	200	-	-	75	60
Cool-down	-	9	890↘200	200	-	1500	200	-

formed the growth of the sensitive film at the highest recommended substrate temperature (890°C) for our CC RF-PECVD tool.

The high growth temperature of NCG does not enable direct deposition on a flexible substrate, as is possible in the case of metal-based commercial strain gauges. Therefore, an optimal probing of the target strain requires transferring the carbon layer on the polymeric film. The usual transfer processes are based on additional supporting/sacrificial layers and chemical etching [10]. To avoid some usual drawbacks-such as chemical residues or wrinkle and crack formation [37] – we explored here an alternative technique based on dry-etching.

In this work we present our first results with developing high-sensitivity piezoresistive elements by employing a capacitively coupled RF-PECVD process to grow high conductivity NCG films on SiO_2/Si substrates and a new film transfer method based on full dry etching of the substrate.

2 Methods and Materials

2.1 Film Growth and Sensor Fabrication

The full workflow for obtaining the final NCG films on flexible substrates is schematically represented in Figure 1. For these experiments we used 4" P/Boron-doped silicon wafers with (100) crystallographic orientation, 1 – 10Ωcm resistivity and a $525 \pm 25 \mu$m thickness, which were thermally oxidized in a Centrotherm 1200 furnace (Centrotherm Systemtechnik GmbH, Germany) in order to grow a ~300 nm thin layer of SiO_2 on the surface. The bulk-NCG deposition was performed by PECVD Nanofab 1000 (Oxford Instruments, UK).

The SiO_2/Si wafer is introduced into the reaction chamber of the RF-PECVD tool at 200°C and gradually heated to 890°C at a rate of 15°C/min in Ar:H_2 atmosphere. After reaching the desired temperature, a H_2 cleaning step in Ar:H_2 atmosphere is performed. The bulk-NCG deposition is accomplished at a pressure of 200 Pa and 100 W RF power in a CH_4:H_2 atmosphere. After the plasma is cut off, the substrate temperature is lowered back to 200°C at 9°C/min and the wafer is evacuated in the loadlock chamber. Before removing the wafer completely, the sample is

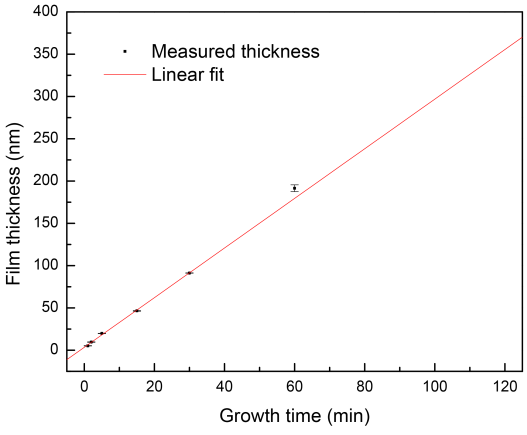

(a)

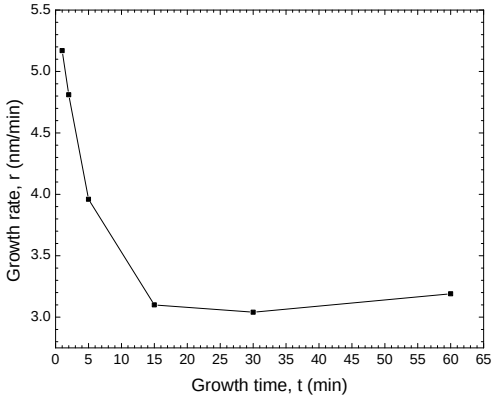

(b)

Figure 2: Dynamics of NCG films growth: (a) thickness and (b) growth rate time-evolutions.

kept for another 10 minutes in the loadlock chamber at 6.6 Pa. The full process, with all the steps and parameters, is presented in Tabular 1. The material thickness and grow rate evolutions are presented in Figure 2. The spectroscopic ellipsometry measurements from [35], on which the growth rate evaluation is based, were accomplished using a SE 800 XUV spectroscopic ellipsometer (Sentech Instruments, Germany) with a laser wavelength of $\lambda = 632$ nm. The 120 minutes growth process reaches an estimated thickness of ~360-380 nm, that was approximated using a two stage extrapolation of the data in Figure 2 (on all available data and on the late slope of the process dynamics).

Before undergoing the transfer process, the NCG film is treated in a low power oxygen plasma using a Plasma Etcher- Etchlab 200 (SENTECH Instruments, Germany) for 5 minutes in order to oversaturate the surface with free oxygen bonds and increase the films' adherence to the flexible substrate. The O_2 plasma was capacitively coupled and ignited at 20 W RF power at a pressure of 20 Pa and an oxygen flow rate of 20 sccm. After the plasma treatment, a thick 2 mm layer of PDMS, which is prepared using a standard 10:1 mixture of base to curing agents, respectively, is applied on the carbon film with the help of a 3D printed polyactide (PLA) mould and left to polymerize at room temperature (RT) and a pressure of ~13×10^3 Pa for 48 hours.

The multilayer structure is etched from the backside as follows: the first SiO_2 layer is etched in a CHF_3:Ar (1:2) atmosphere, at 10 Pa and 350 W RF power for 15 minutes by capacitively coupled RF reactive ion etching, using the Plasma Etcher- Etchlab 200 (SENTECH Instruments, Germany); The Si wafer and the SiO_2 layer next to the NCG thin film are etched in pure SF_6 inductively coupled plasma (ICP) ignited at 0.8 Pa pressure and 1200 W RF power by Plasmalab System 100- ICP Deep Reactive Ion Etching System (Oxford Instruments, UK). After the plasma is stabilized (~5 s), the pressure is increased to 2.66 Pa, and the full Si wafer is etched in a continuous plasma for ~4 hours. The process has a high Si etch rate of ~2.2 µm/min, and the SiO_2 provides a stopping barrier, as the SF_6 plasma selectivity between the two is relatively high (Si:SiO_2=40:1) [38]. The last 50 μm of Si and the SiO_2 layer are etched in steps of 10 and 5 minutes respectively, in order to visually inspect the progress and prevent over etching. The residual SiO_2 can be cleaned in a buffered hydrofluoric acid (BHF) solution for ~1 minute. After the complete etch and successful transfer of the NCG thin film onto the new PDMS substrate, it is diced in strips for mechanoelectrical characterizations (Figure 3). We noticed that the as-grown film uniformity was deteriorated at the ICP etching phase. The significant radial non-uniformity of the transferred film reflects a typical issue with longer ICP etching processes, caused by inhomogeneities of the magnetic field, pressure, reactive species flux. Further optimization of the ICP operating conditions will allow reducing this effect.

The NCG thin film was mechanically contacted with a 1 × 1 cm Cu foil at each end of the strip. After conductive wires were attached to the Cu foils, they were mechanically pressed onto the NCG film in a 3D printed PLA mould, as shown in Figure 4a. The entirety of the contacted NCG film was then encapsulated with PDMS, which is prepared in the same manner as previously explained. The encapsulated device is shown in Figure 4b. The sensors are then

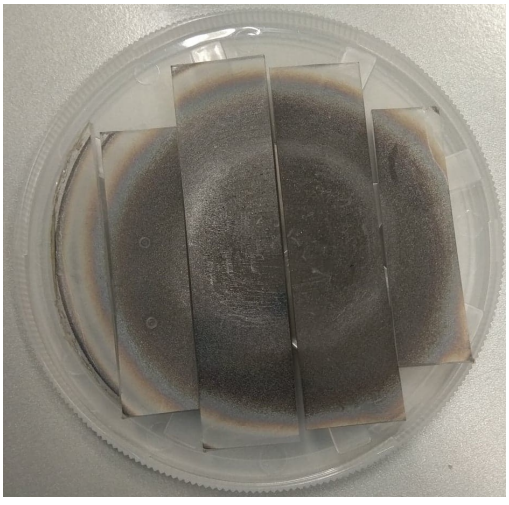

Figure 3: Diced strips of successfully transferred NCG/PDMS

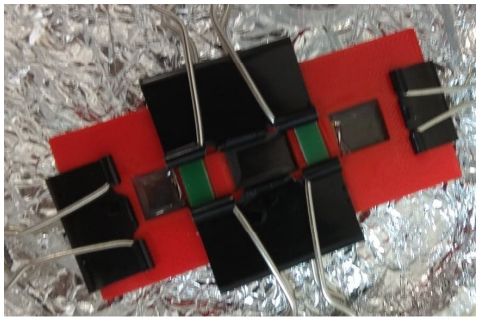

(a)

(b)

Figure 4: (a) NCG/PDMS in PLA mould before encapsulation; (b) NCG/PDMS after complete PDMS encapsulation

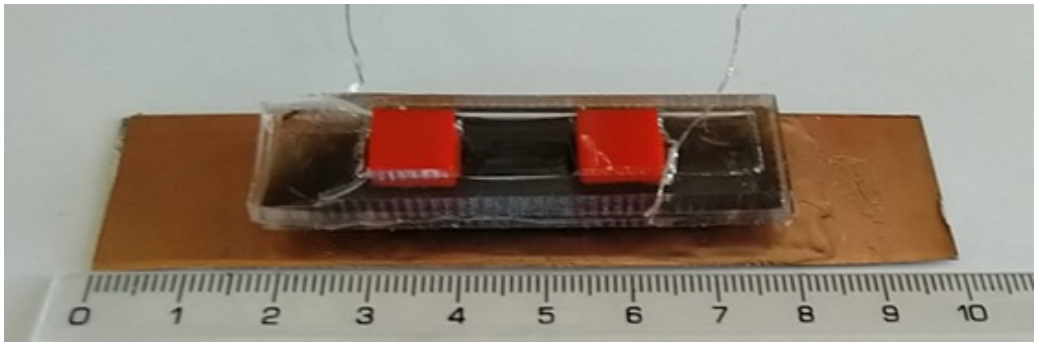

Figure 5: PDMS/NCG/PDMS sample used for electromechanical testing (ruler scale in cm)

glued to an elastic substrate (sticlotextolite), as presented in Figure 5, which is used only for a guiding role in the 3-point bending piezoresistive tests.

2.2 Characterization

Raman spectroscopy measurements were carried out by a high resolution Scanning Near-Field Optical Microscope fitted with the Raman Module Witec Alpha 300S (Witec, Germany) before the O_2 plasma treatment, in order to confirm the type of the obtained carbonic material. The spectra were acquired at 532 nm wavelength.

The conductivity of the as-grown films was measured using a 4200-SCS/C/Keithley instrument (Keithley Instruments, USA) coupled to an Easyprobe EP4 wafer prober (Suss MicroTec, Germany), both on a transmission line measurement (TLM) structure, and by the 4-point van der Pauw method.

The controlled mechanical deformation by 3-point bending was performed with the MultiTest 2.5-i (Mecmesin, UK) equipment, with a distance of 70 mm between the supporting pins. The electrical measurements were realized with a precision multimeter 8846A (Fluke, USA).

3 Results and discussion

The Raman spectroscopy analysis presented in Figure 6 reveals the typical relatively sharp G and D peaks, specific to the NCG class. The sp^2 discontinuities and disorder, as well as the turbostratic stacking, are reflected by the blue shift of the G peak from its ideally graphitic value of 1580 cm^{-1}, by the full width at half maximum (FWHM) values of the main peaks (~67.23 cm^{-1} and 71.91 cm^{-1}, for D and G, respectively) and by the presence of the defect related D+D' peak, while the position and configuration of the 2D peak additionally confirm the turbostratic nature of the material [39, 40]. The dominant interlayer spacing derived from these drifted quantities results of d_{002} ~3.5 Å [39], that is identical with the X-ray diffraction derived value [24, 25]. A rough approximation of an equivalent lateral size of the average crystallite (L_a) in the material can be calculated based on the I_D/I_G intensity ratio of the main peaks. Applying Equation 1 [41] for the measured ratio of ~2.23 and for the laser wavelength (λ_l = 532 nm), an equivalent L_a ~9 nm is obtained.

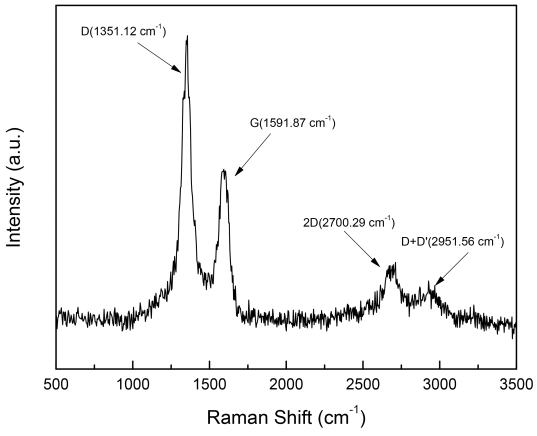

Figure 6: Raman spectrum for bulk-NCG thin film grown on 300 nm thick thermal SiO_2

$$L_a = (2.4 \times 10^{-10})\lambda_l^4 \left(\frac{I_D}{I_G}\right)^{-1} \quad (1)$$

According to the tunneling model proposed by Zhao et al. [10, 18], charge carriers have to resort to tunneling through grain boundaries in order to move from one nanodomain to another, and the piezoresistive effect in bulk-NCG films comes from the variation of the total tunneling distance when the film is subjected to mechanical deforma-

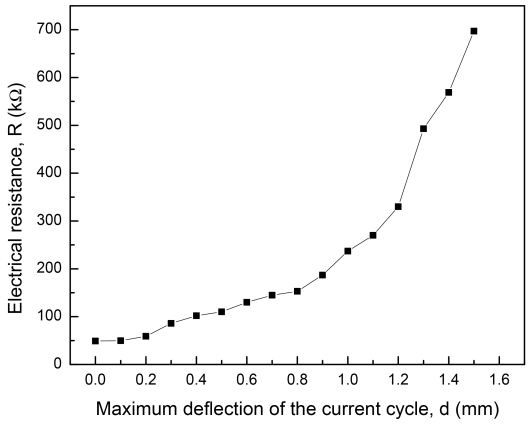

Figure 7: Electrical resistance, R, measured at different maximum deflection values

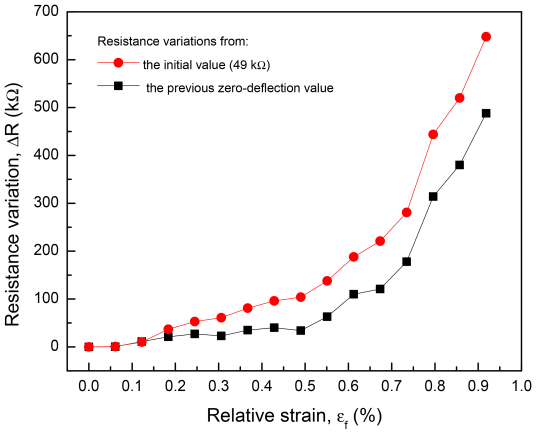

Figure 8: Resistance variations, ΔR, with respect to the strain, ε_f, at the end of each displacement cycle

tion. Due to that fact, bulk-NCG thin films have the capability to modify their GF by changing the growth morphology [10, 18]. That, coupled with the inherent stability of carbonic materials makes bulk-NCG a very promising material for piezoresistive sensors in hostile media.

The electrical conductivity measurements by the TLM and the van der Pauw methods provided similar results ($9.5 - 10.9 \times 10^3$ S/m by TLM, and $9.9 - 10.1 \times 10^3$ S/m by van der Pauw), showing that the as-grown bulk-NCG film has a conductivity of ~10^4 S/m.

A first piezoresistive response test was made through successive 3-point bending deformations and returns to zero deflection, such that in each cycle the targeted maximum deflection at the center of the beam (d) is deeper with 0.1 mm than in the previous cycle, until a final d of 1.5 mm. At the beginning and end of each cycle a resistance measurement was performed. The initial measured value of the sample resistance was 49 kΩ and the up and down displacement rate was 1 mm/min. Figure 7 presents the values measured in this experiment. The piezoresistive sensitivity was calculated with the GF formula:

$$GF(l) = \frac{\frac{\Delta R(l)}{R(l_0)}}{\varepsilon_f(l)} = \frac{R(l) - R(l_0)}{R(l_0)} \cdot \frac{1}{\varepsilon_f(l)} \qquad (2)$$

where $\varepsilon_f(l)$ is the flexural strain and $R(l)$, $R(l_0)$ are the electrical resistances measured in a deformed and relaxed state, respectively. The strain ε_f is calculated by the formula: $\varepsilon_f = \frac{6dt}{L^2}$, where d is the deflection, t is the depth of the sensitive NCG layer relative to the central bending pin (~5 mm) and L is the distance between the two supporting pins (~70 mm).

The measurements revealed a hysteretic behavior of the sensor (Figure 8), most probably due to mechanical delay of the substrates used and possibly other PDMS-NCG interface issues. In Figure 9 we present the effective GF values, that is, those that report the resistance to the less advantageous value, measured at the beginning of the current cycle (previous zero-deflection value). We observe promisingly large values of the GF, but elucidating their relatively large variation and inconsistent trend with the strain needs further development with a thinner and stiffer gauge substrate.

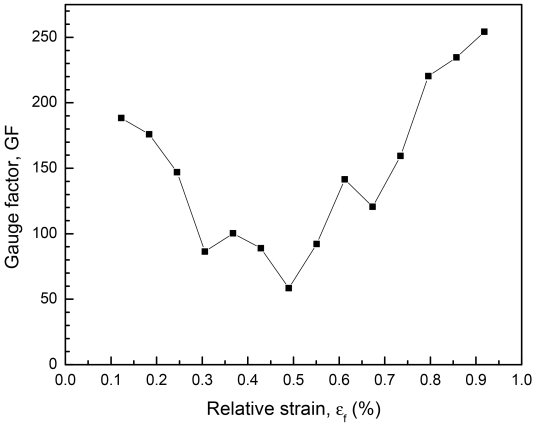

Figure 9: Gauge factor with respect to the relative strain, ε_f, while accounting for the temporal hysteresis

4 Conclusions

In this work we successfully obtained thin films of bulk-NCG, high conductivity turbostratic carbon, by RF-PECVD growth using a CH_4:H_2 gas mixture and developed a reproducible, dry-etching based method for transferring the film on flexible PDMS substrates in order to test its effectiveness for applications requiring high-sensitivity, low-strain sensing.

We presented here our first results in this development, where promising sensitivity values were measured (GF of 50 – 250). Importantly, this level of strain sensitivity was obtained with low-resistance (i.e. thick film) samples, that is essential for viable strain gauges in order to provide enhanced immunity to noise pick-up. The intimate structure of the material is not elucidated, and so is also its actual mechanism of piezorezistivity response.

Future work will pursue both material modification studies - from which we envisage to learn more also on its strain sensitivity mechanism - and improving the transfer process and the sensor construction by using alternative solutions for the polymeric substrate.

Acknowledgement: The authors would like to acknowledge the financial support from the PN-III-P1-1.2-PCCDI-2017-0619 project "Nanostructured carbonic materials for advanced industrial applications" and PN-III-P1-1.2-PCCDI-2017-0637/ 33 PCCDI project "MultiMonD2".

References

[1] Smerd, R., S. Winkler, C. Salisbury, M. Worswick, D. Lloyd, and M. Finn. High strain rate tensile testing of automotive aluminum alloy sheet. *International Journal of Impact Engineering*, Vol. 32, No. 1, 2005, pp. 541–560.

[2] Kouroussis, G., C. Caucheteur, D. Kinet, G. Alexandrou, O. Verlinden, and V. Moeyaert. Review of trackside monitoring solutions: from strain gages to optical fibre sensors. *Sensors*, Vol. 15, No. 8, 2015, pp. 20115–20139.

[3] S. Luo, P. T. Hoang, and T. Liu, "Direct laser writing for creating porous graphitic structures and their use for flexible and highly sensitive sensor and sensor arrays," *Carbon*, vol. 96, pp. 522 – 531, 2016.

[4] A. A. Barlian, W. Park, J. R. Mallon, A. J. Rastegar, and B. L. Pruitt, "Review: Semiconductor piezoresistance for microsystems," *Proceedings of the IEEE*, vol. 97, no. 3, pp. 513–552, 2009.

[5] C. Pang, G.-Y. Lee, T.-i. Kim, S. M. Kim, H. N. Kim, S.-H. Ahn, and K.-Y. Suh, "A flexible and highly sensitive strain-gauge sensor using reversible interlocking of nanofibres," *Nature Materials*, vol. 11, pp. 795–801, Sep 2012.

[6] S. W. Lee, J. J. Park, B. H. Park, S. C. Mun, Y. T. Park, K. Liao, T. S. Seo, W. J. Hyun, and O. O. Park, "Enhanced sensitivity of patterned graphene strain sensors used for monitoring subtle human body motions," *ACS Applied Materials & Interfaces*, vol. 9, no. 12, pp. 11176–11183, 2017. PMID: 28233491.

[7] L.-Q. Tao, D.-Y. Wang, H. Tian, Z.-Y. Ju, Y. Liu, Y. Pang, Y.-Q. Chen, Y. Yang, and T.-L. Ren, "Self-adapted and tunable graphene strain sensors for detecting both subtle and large human motions," *Nanoscale*, vol. 9, pp. 8266–8273, 2017.

[8] Carvalho, A. F., A. J. S. Fernandes, C. Leitao, J. Deuermeier, A. C. Marques, R. Martins, et al. Laser induced graphene strain sensors produced by ultraviolet irradiation of polyimide. *Advanced Functional Materials*, Vol. 28, No. 52, 2018, id. 1805271.

[9] Wang, X., L. Dong, H. Zhang, R. Yu, C. Pan, and Z. L. Wang. Recent progress in electronic skin. *Advanced Science*, Vol. 2, No. 10, 2015, id. 1500169.

[10] J. Zhao, G. Wang, R. Yang, X. Lu, M. Cheng, C. He, G. Xie, J. Meng, D. Shi, and G. Zhang, "Tunable piezoresistivity of nanographene films for strain sensing," *ACS Nano*, vol. 9, no. 2, pp. 1622–1629, 2015. PMID: 25658857.

[11] S. Chen, Y. Wei, X. Yuan, Y. Lin, and L. Liu, "A highly stretchable strain sensor based on a graphene/silver nanoparticle synergic conductive network and a sandwich structure," *J. Mater. Chem. C*, vol. 4, pp. 4304–4311, 2016.

[12] Y. Lee, S. Bae, H. Jang, S. Jang, S.-E. Zhu, S. H. Sim, Y. I. Song, B. H. Hong, and J.-H. Ahn, "Wafer-scale synthesis and transfer of graphene films," *Nano Letters*, vol. 10, no. 2, pp. 490–493, 2010. PMID: 20044841.

[13] Y. Wang, R. Yang, Z. Shi, L. Zhang, D. Shi, E. Wang, and G. Zhang, "Super-elastic graphene ripples for flexible strain sensors," *ACS Nano*, vol. 5, no. 5, pp. 3645–3650, 2011. PMID: 21452882.

[14] Kim, Y.-J., J. Y. Cha, H. Ham, H. Huh, D.-S. So, and I. Kang. Preparation of piezoresistive nano smart hybrid material based on graphene. *Current Applied Physics*, Vol. 11, No. 1, Supplement, 2011, pp. S350–S352.

[15] M. Huang, T. A. Pascal, H. Kim, W. A. Goddard, and J. R. Greer, "Electronic - mechanical coupling in graphene from in situ nanoindentation experiments and multiscale atomistic simulations," *Nano Letters*, vol. 11, no. 3, pp. 1241–1246, 2011. PMID: 21309539.

[16] Casiraghi, C., M. Macucci, K. Parvez, R. Worsley, Y. Shin, F. Bronte et al. Inkjet printed 2D-crystal based strain gauges on paper. *Carbon*, Vol. 129, 2018, pp. 462–467.

[17] C. Stampfer, A. Jungen, R. Linderman, D. Obergfell, S. Roth, and C. Hierold, "Nano-electromechanical displacement sensing based on single-walled carbon nanotubes," *Nano Letters*, vol. 6, no. 7, pp. 1449–1453, 2006. PMID: 16834427.

[18] J. Zhao, C. He, R. Yang, Z. Shi, M. Cheng, W. Yang, G. Xie, D. Wang, D. Shi, and G. Zhang, "Ultra-sensitive strain sensors based on piezoresistive nanographene films," *Applied Physics Letters*, vol. 101, no. 6, p. 063112, 2012.

[19] J. Sun, M. E. Schmidt, M. Muruganathan, H. M. H. Chong, and H. Mizuta, "Large-scale nanoelectromechanical switches based on directly deposited nanocrystalline graphene on insulating substrates," *Nanoscale*, vol. 8, pp. 6659–6665, 2016.

[20] S. J. Fishlock, S. J. O'Shea, J. W. McBride, H. M. H. Chong, and S. H. Pu, "Fabrication and characterisation of nanocrystalline graphite MEMS resonators using a geometric design to control buckling," *Journal of Micromechanics and Microengineering*, vol. 27, p. 095015, aug 2017.

[21] Schmidt, M. E., C. Xu, M. Cooke, H. Mizuta, and H. M. H. Chong. Metal-free plasma-enhanced chemical vapor deposition of large area nanocrystalline graphene. *Materials Research Express*, Vol.

1, No. 2, 2014, id. 025031.

[22] Fishlock S., D. Grech, J. McBride, H. Chong, and S.-H. Pu. Mechanical characterisation of nanocrystalline graphite using micromechanical structures. *Microelectronic Engineering*, Vol. 159, 2016, pp. 184–189.

[23] A. Bianco, H.-M. Cheng, T. Enoki, Y. Gogotsi, R. H. Hurt, N. Koratkar, T. Kyotani, M. Monthioux, C. R. Park, J. M. Tascon, and J. Zhang, "All in the graphene family – a recommended nomenclature for two-dimensional carbon materials," *Carbon*, vol. 65, pp. 1 – 6, 2013.

[24] Albu, C., S. A. V. Eremia, M. L. Veca, A. Avram, R. C. Popa, C. Pachiu et al. Dataset on large area nano-crystalline graphite film (NCG) grown on SiO_2 using plasma-enhanced chemical vapour deposition. *Data in Brief*, Vol. 24, 2019, id. 103923

[25] Albu, C., S. A. Eremia, M. L. Veca, A. Avram, R. C. Popa, C. Pachiu, et al. Nanocrystalline graphite film on SiO2: Electrochemistry and electroanalytical application. *Electrochimica Acta*, Vol. 303, 2019, pp. 284–292.

[26] Transmission electron microscopy analysis of low-roughness (glassy) NCG and of nanowall-surface NCG (graphene nanowalls) carbonic films grown using CC RF-PECVD at IMT Bucharest (to be published, not yet in press).

[27] Simionescu, O.-G., R. C. Popa, A. Avram, and G. Dinescu. Thin films of nanocrystalline graphene/graphite: an overview of synthesis and applications. *Plasma Processes and Polymers*, 2020, id. e1900246, https://doi.org/10.1002/ppap.201900246.

[28] H. Busta, R. Espinosa, A. Rakhimov, N. Suetin, M. Timofeyev, P. Bressler, M. Schramme, J. Fields, M. Kordesch, and A. Silzars, "Performance of nanocrystalline graphite field emitters," *Solid-State Electronics*, vol. 45, no. 6, pp. 1039 – 1047, 2001.

[29] R. C. Mani, M. K. Sunkara, R. P. Baldwin, J. Gullapalli, J. A. Chaney, G. Bhimarasetti, J. M. Cowley, A. M. Rao, and R. Rao, "Nanocrystalline graphite for electrochemical sensing," *Journal of The Electrochemical Society*, vol. 152, no. 4, p. E154, 2005.

[30] D. Noll, P. Hönicke, Y. Kayser, S. Wagner, B. Beckhoff, and U. Schwalke, "Transfer-free in situ CCVD grown nanocrystalline graphene for sub-PPMV ammonia detection," *ECS Journal of Solid State Science and Technology*, vol. 7, no. 7, pp. Q3108–Q3113, 2018.

[31] Z. Zhang, Y. Guo, X. Wang, D. Li, F. Wang, and S. Xie, "Direct growth of nanocrystalline graphene/graphite transparent electrodes on si/sio2 for metal-free schottky junction photodetectors," *Advanced Functional Materials*, vol. 24, no. 6, pp. 835–840, 2014.

[32] Q. Zhang, L. Tang, J. Luo, J. Zhang, X. Wang, D. Li, Y. Yao, and Z. Zhang, "Direct growth of nanocrystalline graphene/graphite all carbon transparent electrode for graphene glass and photodetectors," *Carbon*, vol. 111, pp. 1 – 7, 2017.

[33] Rana, S., J. D. Reynolds, T. Y. Ling, M. S. Shamsudin, S. H. Pu, H. M. Chong, et al. Nano-crystalline graphite for reliability improvement in MEM relay contacts. *Carbon*, Vol. 133, 2018, pp. 193–199.

[34] Fishlock, S., S. Pu, G. Bhattacharya, Y. Han, J. McLaughlin, J. McBride, et al. Micromachined nanocrystalline graphite membranes for gas separation. *Carbon*, Vol. 138, 2018, pp. 125–133.

[35] Simionescu, O.-G., E. Anghel, R. C. Popa, C. Pachiu, R. Gavrilă, F. Comănescu, et al. Bulk nanocrystalline graphite thin films for piezorezistive sensing applications. Proceedings of the *International Semiconductor Conference (CAS)*, October 9–11, 2019, Sinaia, Romania, *IEEE Xplore* 2020 pp. 229–232.

[36] D. Liu, W. Yang, L. Zhang, J. Zhang, J. Meng, R. Yang, G. Zhang, and D. Shi, "Two-step growth of graphene with separate controlling nucleation and edge growth directly on sio2 substrates," *Carbon*, vol. 72, pp. 387 – 392, 2014.

[37] Ma, L.-P., W. Ren, and H.-M. Cheng. Transfer methods of graphene from metal substrates: A review. *Small Methods*, Vol. 3, No. 7, 2019, id. 1900049.

[38] d'Agostino, R., and D. L. Flamm. Plasma etching of Si and SiO_2 in SF_6-O_2 mixtures. *Journal of Applied Physics*, Vol. 52, No. 1, 1981, pp. 162–167.

[39] Lespade, P., A. Marchand, M. Couzi, and F. Cruege. Caracterisation de materiaux carbones par microspectrometrie raman. *Carbon*, Vol. 22, No. 4, 1984, pp. 375–385.

[40] A. C. Ferrari and D. M. Basko, "Raman spectroscopy as a versatile tool for studying the properties of graphene," *Nature Nanotechnology*, vol. 8, pp. 235–246, Apr 2013.

[41] Cançado, L. G., K. Takai, T. Enoki, M. Endo, Y. A. Kim, H. Mizusaki, et al. General equation for the determination of the crystallite size L_a of nanographite by Raman spectroscopy. *Applied Physics Letters*, Vol. 88, No. 16, 2006, id. 163106.